Observation of Reverse Saturable Absorption of an X-ray Laser

B. I. Cho,[1,2,*] M. S. Cho,[1,2] M. Kim,[1,2] H.-K. Chung,[3] B. Barbrel,[4] K. Engelhorn,[4] T. Burian,[5] J. Chalupský,[5] O. Ciricosta,[6] G. L. Dakovski,[7] V. Hájková,[5] M. Holmes,[7] L. Juha,[5] J. Krzywinski,[7] R. W. Lee,[8] Chang Hee Nam,[1,2] D. S. Rackstraw,[6] S. Toleikis,[9] J. J. Turner,[7] S. M. Vinko,[6] J. S. Wark,[6] U. Zastrau,[10] and P. A. Heimann[7]

[1]*Center for Relativistic Laser Science, Institute for Basic Science (IBS), Gwangju 61005, Korea*
[2]*Department of Physics and Photon Science, Gwangju Institute of Science and Technology, Gwangju 61005, Korea*
[3]*Atomic and Molecular Data Unit, Nuclear Data Section, IAEA, P.O. Box 100, A-1400 Vienna, Austria*
[4]*Lawrence Berkeley National Laboratory, 1 Cyclotron Road, Berkeley, California 94720, USA*
[5]*Institute of Physics ASCR, Na Slovance 2, 18221 Prague 8, Czech Republic*
[6]*Department of Physics, Clarendon Laboratory, University of Oxford, Parks Road, Oxford OX1 3PU, United Kingdom*
[7]*SLAC National Accelerator Laboratory, 2575 Sand Hill Road, Menlo Park, California 94025, USA*
[8]*Department of Physics, University of California, Berkeley, California 94720, USA*
[9]*Deutsches-Elektronensynchrotron DESY, Notkestrasse 85, D-22603 Hamburg, Germany*
[10]*European XFEL, Holzkoppel 4, 22869 Schenefeld, Germany*

(Received 19 December 2016; revised manuscript received 18 May 2017; published 16 August 2017)

A nonlinear absorber in which the excited state absorption is larger than the ground state can undergo a process called reverse saturable absorption. It is a well-known phenomenon in laser physics in the optical regime, but is more difficult to generate in the x-ray regime, where fast nonradiative core electron transitions typically dominate the population kinetics during light matter interactions. Here, we report the first observation of decreasing x-ray transmission in a solid target pumped by intense x-ray free electron laser pulses. The measurement has been made below the K-absorption edge of aluminum, and the x-ray intensity ranges are 10^{16}–10^{17} W/cm^2. It has been confirmed by collisional radiative population kinetic calculations, underscoring the fast spectral modulation of the x-ray pulses and charge states relevant to the absorption and transmission of x-ray photons. The processes shown through detailed simulations are consistent with reverse saturable absorption, which would be the first observation of this phenomena in the x-ray regime. These light matter interactions provide a unique opportunity to investigate optical transport properties in the extreme state of matters, as well as affording the potential to regulate ultrafast x-ray free-electron laser pulses.

DOI: 10.1103/PhysRevLett.119.075002

Reverse saturable absorption (RSA), i.e., the increase in the light absorption with increasing intensity, is a well-known nonlinear phenomenon in optical science [1–7]. A light absorber whose excited state absorption is larger than the ground state can undergo this effect. Typically, at high intensities, materials that exhibit RSA and/or two-photon absorption are of importance for applications such as two-photon microscopy, optical switching, laser pulse shaping, and compression, and upconversion lasing [8–10].

In the x-ray regime, the impressive progress in developing x-ray free electron lasers (XFEL) over the last several years has made it possible to produce x-ray intensities exceeding 10^{17} W/cm^2, and enabled new investigations of x-ray–matter interactions [11–13]. A series of investigations have shown that XFEL pulses are intense enough to deliver multiple photons to each atom, even in solid-density samples, in the tens-of-femtosecond time scale leading to nonlinear phenomena [14–18]. One of the noticeable effects reported was saturable absorption (SA) in aluminum and iron [19,20]. In both cases, an increase of the x-ray transmission at high intensity was observed near and above the K-absorption edge of each element.

While it has long been known that the x-ray opacity of matter can be modified by heating and ionizing it on nanosecond time scales [21–24], the RSA of a monochromatic x-ray source has yet to be reported. In this Letter, we demonstrate the decreased x-ray transmission through the sample with increasing x-ray intensity. The observation was made around 1487 eV below the K-absorption edge (1560 eV) of aluminum and XFEL intensities were in the range of 10^{16}–10^{17} W/cm^2. Collisional-radiative calculations exhibit good agreement with the experimental data. These calculations provide detailed charge state population kinetics and physical insight into the XFEL-matter interaction at high intensities. The decreased x-ray transmission can be explained by the creation and annihilation of the highly absorptive but short-lived excited state via a sequential multiphoton absorption process. This process is consistent with the RSA mechanism in the optical regime. It modulates the XFEL pulse in both the spectral and temporal domains. Finally, a possible transition from RSA to SA at even higher intensities is discussed.

The experiment was performed at the Soft X-ray Material Science (SXR) Instrument of the Linac

Coherent Light Source (LCLS) [25–27]. The x-ray beam in self-amplified spontaneous emission (SASE) mode, which have an energy bandwidth of ~0.3%, was set in the photon energy range between 1480 and 1510 eV, which lies well below the K edge of aluminum. The x rays were focused to an effective area of 7 μm^2 using a pair of Kirkpatrick-Baez mirrors, and incident on a 1 μm thick aluminum foil supported by a fine nickel mesh, which covers ~10% of the target surface area, with an angle of incidence of 45°. As the foil was translated after each shot to expose a fresh surface, ~10% of data might not show the true transmission due to the total or partial block of x-ray beam by the mesh. It could contribute to the increase of experimental error.

With a nominal pulse duration of 100 fs, pulse energy of 2 mJ at the gas monitor detector (GMD) and a beam line transmission of ~34% [28], a peak intensity of 10^{17} W/cm^2 was achieved on the target. The x-ray transmission was determined based on the simultaneous pulse energy measurement at the GMD upstream in the beam line and at a photodiode behind the sample. In order to prevent saturation of a diode by high pulse energies, a heavy attenuation (~10^4) was applied using carbon filters, which has a smooth transmission profile in the photon energy range of the experiment. A heavy attenuation introduced the large fluctuations with respect to the small signals, particularly for the low pulse energy measurement (<1 mJ). The uncertainty of incident pulse energy measurement at the GMD [28] also contributed to the experimental errors. More details of the experimental setup are given in the work of Rackstraw *et al.* [19].

Figure 1 shows the measured x-ray transmission for various pulse energies as a function of incident photon energy. First, the photon energy of low energy pulses (<0.5 mJ at GMD) was scanned in the range of 1475–1510 eV. The corresponding peak intensities were lower than 2×10^{16} W/cm^2. Each data point represents a single shot measurement. Although there is large scatter in the data, a reasonable agreement with the cold Al transmission was found over the whole range [29].

Then, the nominal x-ray photon energy was set to 1487 eV. The pulse energy was increased to 2.5 mJ at the GMD, and a peak intensity of 1×10^{17} W/cm^2 was achieved. While there is some shot-to-shot variation in the recorded XFEL photon energies (1485–1490 eV) and transmissions, a clear trend of the reduction in transmission as a function of intensity was observed. With the maximum pulse energies (>2 mJ at the GMD), the transmission dropped below 60%. Compared with the typical absorption value at 1487 eV (~14%) [29], this corresponds to a threefold enhancement in the absorption. This behavior shows a clear signature of RSA. Considering the high intensity, such x-ray absorption can lead to a rapid heating of the sample and the creation of a hot, solid-density plasma [18].

The interaction of the XFEL pulses with the aluminum foil was modeled using the collisional-radiative population

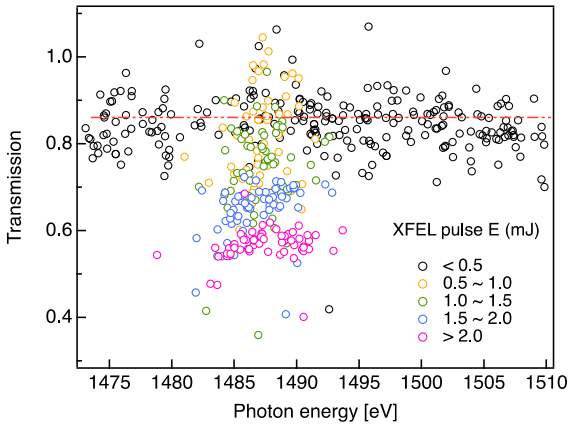

FIG. 1. Measurement of x-ray transmission through an aluminum foil target. Each circle represents the data from a single shot. The red line is the known transmission value of cold Al from the CXRO database. The peak intensities of the highest pulse energies (pink circles) correspond to ~10^{17} W/cm^2.

kinetics code SCFLY [30], which has been shown previously to be successful in simulating the conditions produced in such high intensity x-ray–matter interactions [17–19, 31–33]. The XFEL pulse duration, central photon energy, and bandwidth is set to 100 fs, 1490 eV, and 0.3%, respectively. The peak intensities were varied from 1×10^{15} to 1×10^{18} W/cm^2. The Al sample thickness is set to be 1.4 μm, considering the incidence angle of x-ray beam. The x-ray penetration depth is strongly dependent on the intensity, and the sample is not irradiated uniformly through the sample depth. This effect is taken into account by dividing the foil into 10 thin laminae (0.14 μm each), and the transmitted x-ray pulse from the previous lamina is used as an incident pulse on the following one. The intensity distribution of the XFEL focal spot is also taken into account. With a given peak intensity, the total transmission and absorption are determined by an area-weighted sum of the various intensities in the focal spot.

Figure 2 shows the calculated XFEL spectrum as it propagates through the aluminum foil for several different intensities. At a low intensity (10^{16} W/cm^2), the intensity decreases progressively but slightly through the sample, with little or no change in spectral shape. As a result, a flat, low, transmission across the spectral range is obtained [Fig. 2(b)], which corresponds to that observed for a cold aluminum sample. The absorption is due to the well-known L-shell photoionization ($\sigma_{2p} = 7 \times 10^{-3}$ Mb/atom) [34]. The result agrees well with the cold transmission curve as well as the low-intensity measurements (black circles in Fig. 1).

Figure 2(a) illustrates that above 10^{16} W/cm^2, a dip in the spectrum near 1487 eV appears, which gets deeper as the pulse propagates through the sample. The width (~1 eV FWHM) of this dip is narrower than the typical LCLS bandwidth (~5 eV) [Fig. 2(b)]. At 1×10^{17} W/cm^2, this hole is the deepest and almost ~80% of 1487 eV photons

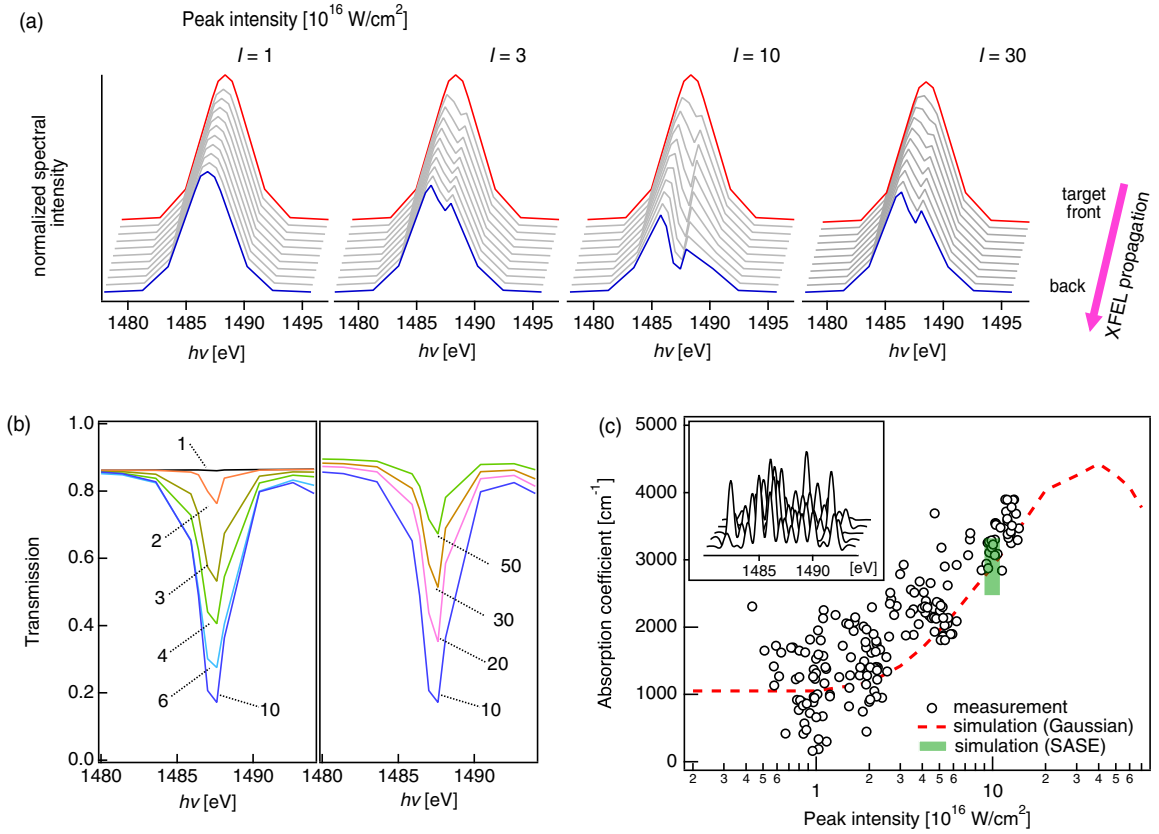

FIG. 2. (a) Simulation of transmitted x-ray spectra through an aluminum sample at selected intensities (1, 3, 10, 30×10^{16} W/cm^2). The incident and final transmitted spectra are depicted in the red and blue curves. The sample is divided into 10 laminae, and the transmission after each lamina is shown in gray. Each curve is normalized to the highest spectral intensity of the incident spectrum. (b) Final transmission spectra, obtained by the blue divided by the red curves in (a), for $I = 1$–50×10^{16} W/cm^2. (c) Absorption coefficient of aluminum as a function of peak intensity. The circles represent the experimental data at 1485–1490 eV. The dashed line is the theoretical prediction from SCFLY. Note the intensity in (a) and (b) is at a single value without considering the intensity distribution of the XFEL focal spot. But in (c), the calculation includes the intensity distribution of the focal spot. Inset: Some simulation of transmitted SASE spectra. The incident spectra are corresponding to Gaussian profiles of 100 fs and 5 eV FWHM and a peak intensity of $\sim 1 \times 10^{17}$ W/cm^2. In the main plot, the range of calculated absorption of 100 SASE pulse is shown as a green box.

are absorbed. It is noted that 1487 eV corresponds to the Al $K\alpha$ emission energy, indicating a resonance with $1s - 2p$ transitions. The off-resonant photons in the same XFEL pulse are not absorbed as much as the resonant ones.

In Fig. 2(c), the absorption coefficients, $\mu = -1/d \ln(T)$ are plotted as a function of peak x-ray intensity, where d is the sample thickness and T the transmission. Black circles correspond to the transmission data at 1485–1490 eV shown in Fig. 1. In order to make a direct comparison with experiment, two considerations are made in the calculations. First, the absorption (transmission) is obtained by the spectral integration of curves in Fig. 2(b). Second, the intensity distribution of the x-ray focus is taken into account. With a given peak XFEL intensity, the absorption for various intensities is area weighted and averaged. Figure 2(c) shows that in the peak intensity range of $10^{16} \times 10^{17}$ W/cm^2 the typical behavior of RSA is well reproduced and that the simulation agrees with the observed experimental trends.

It is interesting to note that at higher intensity ($>2 \times 10^{17}$ W/cm^2) the simulation predicts more transmission than at 1×10^{17} W/cm^2; i.e., a transition from RSA to SA might occur. In order to observe such an effect in the experiment, a reasonable fraction of the XFEL focal area should have high enough intensity. Therefore, as shown in Fig. 2(c), the transition is predicted to appear at a peak intensity around 5×10^{17} W/cm^2. Although experiments at such high intensities are not yet possible in the soft x-ray regime, such a transition would be quite interesting, given the implications for potentially being able to manipulate XFEL pulses.

It is also noted that the Gaussian spectral and temporal profiles of XFEL pulses were assumed in the simulations. In order to check the validity of this assumption, simulations using SASE pulses were also performed. In the inset of Fig. 2(c), a few examples of transmitted SASE spectra corresponding to the incident peak intensity of 1×10^{17} W/cm^2 are shown. Overall low transmissions near

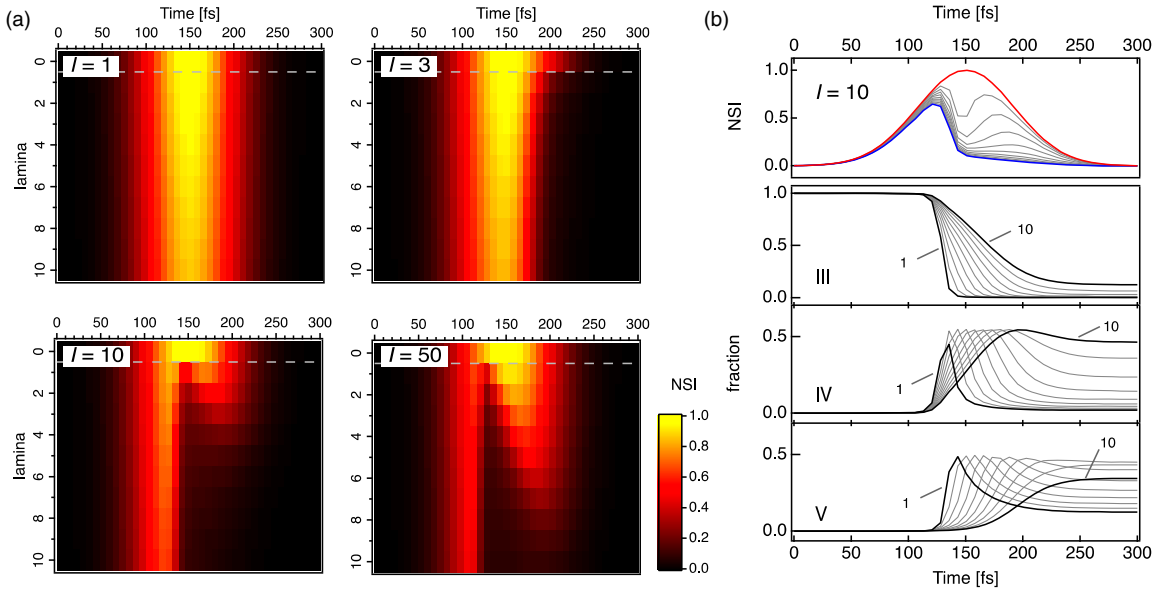

FIG. 3. (a) Temporal evolution of the spectral intensity (SI) of the resonant x-ray photons through each lamina. Lamina "0" above the dashed line represents the incident x-ray pulse. The SI is normalized to the peak value of each incident pulse. (b) For the case of 1×10^{17} W/cm^2, the top panel shows the SI through each lamina, and the second to fourth panels display the temporal evolution of the charge state (CS) III–V at each lamina. The first (1) and the last (10) laminas are plotted with thick solid lines.

the resonance are observed. The absorptions obtained from 100 SASE simulations are marked in Fig. 2(c). An agreement with the Gaussian simulation infers that similar to precedent papers [17–19,31–33], the use of the Gaussian XFEL profile is still valid for this work. The random energy concentration near the resonance introduces a spread in the absorption, and could explain the spread in the measurement.

In order to gain deeper physical insight, the temporal profiles of the XFEL pulse around the resonant photon energy (1486–1488 eV) and the charge states (CS) of the sample were explored. For a clear observation of physical effects, each simulation is performed for a single intensity with the Gaussian profiles, and not averaged over the spot profile.

At a low intensity (10^{16} W/cm^2), from the beginning to the end of the XFEL pulse, a flat transmission is observed at all depths of the foil [Fig. 3(a)]. In fact, this calculation is the same as in Fig. 2(a) at the same intensity, but now shown in the temporal domain. The incident photon areal density is 0.5 of that of the atomic areal density in the target; i.e., during the pulse each atom is on average exposed to 0.5 photons. With a small L-shell photoionization cross section, the sample mostly remains in the ground state (K^2L^8, CS III). Only a very small fraction of L-shell electrons is photoionized to an excited state (K^2L^7, CS IV).

At higher peak intensities, the fall and rise of spectral intensity is observed at various times and within different depths of the sample. In the case of 1×10^{17} W/cm^2, after the first lamina the pulse has a sharp dip in the middle. As the pulse propagates, the second layer of the sample is irradiated with this temporally modulated pulse and introduces further modulations. Finally, after 150 fs resonant photons are barely transmitted through the final layer of the sample.

In Fig. 3(b), the temporal evolution of CS III, IV, and V are depicted together with the spectral intensity at 1×10^{17} W/cm^2. The fractional population of CS III in the first lamina quickly decreases at ~120 fs, and that of CS IV increases. The latter is an excited state created by L-shell photoionization ($K^2L^8 + h\nu \rightarrow K^2L^7$) and more absorptive than the ground state, which is a necessary condition of RSA. The development of CS IV leads to a rapid drop in the x-ray photons ($K^2L^7 + h\nu \rightarrow K^1L^8$). Finally, CS IV decays mainly to CS V (K^2L^6) via the Auger process. Once all CS IV Al atoms reach a higher CS, no further absorption will occur and the system will be bleached, and thus the spectral intensity of the x-ray pulse is restored. A similar process happens in the following lamina with the modulated pulse at a slightly later time. At each depth, the spectral dip in the XFEL pulse is correlated with the population of CS IV. The early part of the XFEL pulse penetrates and can develop a significant population of CS IV at the rear side of the sample. However, the later part of the pulse has been highly absorbed in the front and middle of the sample. At the rear side, the XFEL pulse does not contain enough resonant photons. The CS IV cannot be converted into a higher CS and remains until the end of the simulation.

The simulations for very high intensity (5×10^{17} W/cm^2) indicate that at the rear side of the sample, there are enough resonant photons to deplete all of the CS IV population.

As a result, the resonant photons in the later part of the XFEL pulse can escape the sample. This change explains the transition from RSA to SA. With a further development of XFEL technology, such as higher pulse energies or tighter focusing, this effect should be observable.

Finally, it is noted that Kanter *et al.* showed that although the SASE pulse is temporally incoherent, a strong XFEL pulse can induce Rabi cycling on neon and modify the Auger line shape at the resonant condition [15]. Future investigation with high resolution spectral measurements of x-ray emission and transmission could address such an effect in a solid sample.

In this Letter, we report the first observation of decreasing x-ray transmission of the high intensity XFEL pulse. With an intense XFEL pulse tuned to the K-L resonance, the x-ray transmission through an aluminum foil shows a sharp drop in the intensity range of 10^{16}–10^{17} W/cm^2. At a resonant energy below the K-absorption edge, x-ray absorption can increase as high as in the above edge regime. Using collision-radiative simulations, we discuss the details of the material response at high XFEL intensities as well as the temporal and spectral modulation of the XFEL pulses. These results are consistent with the resonant sequential two-photon absorption within an L-shell lifetime. An exotic material condition is created in which photoexcitation from the K shell and Auger decay from the M shell are competing. The calculations further predict a transition from RSA to SA at higher intensities. RSA and accompanying sequential two-photon absorption are strongly depending on x-ray intensity and could have potential applications, such as characterization of the XFEL focal spot and modulating spatial modes of XFEL beam. It could also impact on future development, such as two-photon fluorescent probes and amplification of x-ray pulses.

This is work was supported by the Institute for Basic Science (IBS-R012-D1) and the National Research Foundation (NRF-2016R1A2B4009631 and NRF-2015R1A5A1009962) of Korea. O. C., D. S. R. and J. S. W. are grateful to the UK EPSRC for support under grants EP/H035877/1 and EP/L000849/1. S. M. V. gratefully acknowledges support for the Royal Society. Use of the LCLS, SLAC National Accelerator Laboratory, is supported by the U.S. Department of Energy, Office of Science, Office of Basic Energy Sciences under Contract Number DE-AC02-76SF00515. The SXR Instrument is funded by a consortium whose membership includes the LCLS, Stanford University through the Stanford Institute for Materials Energy Sciences (SIMES), Lawrence Berkeley National Laboratory (LBNL), University of Hamburg through the BMBF priority programme FSP 301 and the Center for Free Electron Laser Science (CFEL).

*bicho@gist.ac.kr

[1] L. W. Tutt and A. Kost, Nature (London) **356**, 225 (1992).
[2] J. W. Perry *et al.*, Science **273**, 1533 (1996).
[3] P. Chen, X. Wu, X. Sun, J. Lin, W. Ji, and K. L. Tan, Phys. Rev. Lett. **82**, 2548 (1999).
[4] M. O. Senge, M. Fazekas, E. G. A. Notaras, W. J. Blau, M. Zawadzka, O. B. Locos, and E. M. Ni Mhuircheartaigh, Adv. Mater. **19**, 2737 (2007).
[5] G. J. Zhou, W.-Y. Wong, C. Ye, and Z. Lin, Adv. Funct. Mater. **17**, 963 (2007).
[6] Y. Xu, Z. Liu, X. Zhang, Y. Wang, J. Tian, Y. Huang, Y. Ma, X. Zhang, and Y. Chen, Adv. Mater. **21**, 1275 (2009).
[7] G.-K. Lim, Z.-L. Chen, J. Clark, R. G. S. Goh, W.-H. Ng, H.-W. Tan, R. H. Friend, P. K. H. Ho, and L.-L. Chua, Nat. Photonics **5**, 554 (2011).
[8] B. Zhang, Y. Li, R. Liu, T. M. Pritchett, J. E. Haley, and W. Sun, ACS Appl. Mater. Interfaces **5**, 565 (2013).
[9] M. Pawlicki, H. A. Collins, R. G. Denning, and H. L. Anderson, Angew. Chem., Int. Ed. **48**, 3244 (2009).
[10] G. S. He, L.-S. Tan, Q. Zheng, and P. N. Prasad, Chem. Rev. **108**, 1245 (2008).
[11] P. Emma *et al.*, Nat. Photonics **4**, 641 (2010).
[12] T. Ishikawa *et al.*, Nat. Photonics **6**, 540 (2012).
[13] C. Bostedt, S. Boutet, D. M. Fritz, Z. Huang, H. J. Lee, H. T. Lemke, A. Robert, W. F. Schlotter, J. J. Turner, and G. J. Williams, Rev. Mod. Phys. **88**, 015007 (2016).
[14] L. Young *et al.*, Nature (London) **466**, 56 (2010).
[15] E. P. Kanter *et al.*, Phys. Rev. Lett. **107**, 233001 (2011).
[16] K. Tamasaku *et al.*, Nat. Photonics **8**, 313 (2014).
[17] S. M. Vinko *et al.*, Nature (London) **482**, 59 (2012).
[18] B. I. Cho *et al.*, Phys. Rev. Lett. **109**, 245003 (2012).
[19] D. S. Rackstraw *et al.*, Phys. Rev. Lett. **114**, 015003 (2015).
[20] H. Yoneda, Y. Inubushi, M. Yabashi, T. Katayama, T. Ishikawa, H. Ohashi, H. Yumoto, K. Yamauchi, H. Mimura and H. Kitamura, Nat. Commun. **5** (2014).
[21] S. J. Davidson, J. M. Foster, C. C. Smith, K. A. Warburton, and S. J. Rose, Appl. Phys. Lett. **52**, 847 (1988).
[22] T. S. Perry *et al.*, Phys. Rev. Lett. **67**, 3784 (1991).
[23] C. Chenais-Popovics *et al.*, J. Quant. Spectrosc. Radiat. Transfer **65**, 117 (2000).
[24] J. J. MacFarlane *et al.*, Phys. Rev. E **66**, 046416 (2002).
[25] P. Heimann *et al.*, Rev. Sci. Instrum. **82**, 093104 (2011).
[26] W. F. Schlotter *et al.*, Rev. Sci. Instrum. **83**, 043107 (2012).
[27] G. L. Dakovski, P. Heimann, M. Holmes, O. Krupin, M. P. Minitti, A. Mitra, S. Moeller, M. Rowen, W. F. Schlotter, and J. J. Turner, J. Synchrotron Radiat. **22**, 498 (2015).
[28] K. Tiedtke *et al.*, Opt. Express **22**, 21214 (2014).
[29] CXRO, http://www.cxro.lbl.gov.
[30] H. K. Chung, R. W. Lee, and M. H. Chen, High Energy Density Phys. **3**, 57 (2007).
[31] O. Ciricosta, H.-K. Chung, R. W. Lee, and J. S. Wark, High Energy Density Phys. **7**, 111 (2011).
[32] O. Ciricosta *et al.*, Phys. Rev. Lett. **109**, 065002 (2012).
[33] D. S. Rackstraw *et al.*, High Energy Density Phys. **11**, 59 (2014).
[34] http://xdb.lbl.gov.